



**HAL**  
open science

# Experimental study on the effect of mechanical ventilation conditions and fire dynamics on the pressure evolution in an air-tight compartment

Junyi Li, Hugues Pretrel, Sylvain Suard, Tarek Beji, Bart Merci

## ► To cite this version:

Junyi Li, Hugues Pretrel, Sylvain Suard, Tarek Beji, Bart Merci. Experimental study on the effect of mechanical ventilation conditions and fire dynamics on the pressure evolution in an air-tight compartment. *Fire Safety Journal*, 2021, 125, pp.103426. 10.1016/j.firesaf.2021.103426 . hal-03381470

**HAL Id: hal-03381470**

**<https://hal.science/hal-03381470>**

Submitted on 16 Oct 2021

**HAL** is a multi-disciplinary open access archive for the deposit and dissemination of scientific research documents, whether they are published or not. The documents may come from teaching and research institutions in France or abroad, or from public or private research centers.

L'archive ouverte pluridisciplinaire **HAL**, est destinée au dépôt et à la diffusion de documents scientifiques de niveau recherche, publiés ou non, émanant des établissements d'enseignement et de recherche français ou étrangers, des laboratoires publics ou privés.



Distributed under a Creative Commons Attribution - NonCommercial - NoDerivatives 4.0 International License

# Experimental study on the effect of mechanical ventilation conditions and fire dynamics on the pressure evolution in an air-tight compartment

Junyi Li <sup>a</sup>, Hugues Prétrel <sup>b</sup>, Sylvain Suard <sup>b</sup>, Tarek Beji <sup>a</sup>, Bart Merci <sup>a</sup>

<sup>a</sup> Ghent University, Department of Structural Engineering and Building Materials, 9000 Ghent, Belgium

<sup>b</sup> Institut de Radioprotection et de Sûreté Nucléaire (IRSN), Centre de Cadarache, 13115 St Paul Lez Durance, France

## Abstract

The paper presents a comprehensive set of experiments on the effect of mechanical ventilation conditions and fire dynamics on temporal pressure evolution in a reduced-scale, air-tight and mechanically-ventilated enclosure.

A square propane burner with flow controller imposes a quadratic fire growth followed by a steady-state (0.1 or 0.2 g/s) and then a quadratic decay phase. Eight tests are discussed with different ventilation conditions in terms of flow resistances and initial ventilation flow rates ranging from 12 to 40 m<sup>3</sup>/h, corresponding to air renewal rates of 6.4 to 21.3 h<sup>-1</sup>.

The pressure evolution is characterized by an over-pressure peak (up to 900 Pa) followed by a quasi-steady state and then, an under-pressure peak (up to -760 Pa). The pressure variation is due to the mechanical effect (i.e., ventilation configurations), while also influenced by thermal effects. The pressure amplitudes increase with ventilation resistances. Both the total network resistance and individual resistances in admission and extraction ducts are important for the pressure variation. The enhancement and reduction of ventilation flow rates depend on both the fire-induced pressure and ventilation resistances. Experimental results show that the mechanical effect does not strongly affect gas temperatures.

**Keywords:** air-tight compartment fire; mechanical ventilation; pressure; fire dynamics

## 1. Introduction

Air-tight compartments are encountered in both residential and industrial fields. The demand for energy-saving promotes the appearance of air-tight residential buildings, e.g., passive houses [1], to limit the air infiltration, which is responsible for a large amount of energy consumption [2]. Besides, a high confinement level is also applied in industrial constructions such as nuclear power plant buildings to prevent the radioactive substance from leaving the building [3]. The increasing applications of air-tight buildings have aroused the interest in studying fire dynamics in compartments representing these buildings [3-9]. The present paper will mainly focus on the pressure variations in an air-tight compartment with mechanical ventilation in case of a fire event.

Unlike compartments with sufficiently large openings, the fire-induced pressure can rise substantially in air-tight compartments because of the difficulty in releasing hot combustion products and thermal expansion [10]. Experiments carried out in air-tight compartments have revealed an obvious over-pressure during the fire growth period and an under-pressure during the fire decay period in large scale experimental facilities [3, 7, 11] as well as in real residential buildings [5, 6]. Due to the high fire-induced pressure in the experiment, the building structure can even be destroyed [6]. Numerical simulation results also confirm that the indoor pressure

will change significantly due to fire inside an air-tight compartment [5, 6, 12]. The fire-induced pressure is usually ignored in engineering calculations considering the leakage of conventional buildings [10]. However, with the increasing of the airtightness level of buildings, such pressure variation caused by fire should be taken into consideration.

A classical theory to interpret the fire-induced pressure variation is based on the mass and energy conservation [3, 10, 13, 14]:

$$\frac{V}{\gamma - 1} \frac{d}{dt} p = Q_f - Q_v - Q_w \quad (1)$$

where  $p$  is the compartment pressure (Pa),  $V$  is the compartment volume ( $\text{m}^3$ ),  $\gamma$  is the gas isentropic coefficient,  $Q_f$ ,  $Q_v$  and  $Q_w$  represent the fire heat release rate (kW), the ventilation heat transfer (kW) and the wall (boundary) heat losses (kW), respectively. It has been reported that the pressure is mainly influenced by the heat release rate (HRR), ventilation conditions and heat losses through boundaries [3, 13, 14]. This guides the design of the present experimental campaign to systematically investigate the factors affecting fire-induced pressure variation.

In air-tight residential buildings, a mechanical ventilation system is applied to compensate for unintended adverse consequences due to airtightness in daily life [15, 16]. Also, for industrial buildings, like the nuclear power plant, dynamic confinement is acquired by mechanical ventilation to ensure the safety requirements [3, 17]. The ventilation condition has been proven to have an impact on the pressure variation [3, 5]. It is noted that the ventilation flow rates are strongly dependent on the compartment pressure itself in airtight compartments, and this has a strong impact on the pressure dynamics. However, the influence of different ventilation settings, namely ventilation resistances and initial ventilation flow rates, on the pressure evolution has not been studied systematically. Therefore, a parametric study of the influence of ventilation conditions on pressure variation, as part of an extensive experimental campaign, is reported in the present paper. The aim is to shed light on the impact of the total flow resistance, as well as the individual flow resistances in admission and extraction ducts, on the ventilation flow rates, fire dynamics and compartment pressure evolution. Moreover, the experimental data can serve as database for numerical simulations and fire safety analysis.

Before doing the actual fire tests, the compartment airtightness has been estimated through pressurization and depressurization tests to determine the leakage flow rate. Then, test results with different ventilation resistances are analyzed, keeping the initial ventilation flow rate fixed. This is followed by tests with different initial ventilation flow rates. It is important, though, to start with a complete description of the experimental set-up.

## 2. Experimental setup

### 2.1. The compartment

The experiments are performed in an air-tight compartment called NYX of the “Institut de radioprotection et de Sûreté Nucléaire” (IRSN), which is a 1:4 scale of one room of the large-scale DIVA facility also from IRSN [7, 18]. The internal dimensions of the compartment are 1.5 m in length, 1.25 m in width and 1 m in height, resulting in an internal volume of  $1.875 \text{ m}^3$ . The compartment is based on a metallic frame on which rectangular plates corresponding to walls, ceiling and floor are inserted. Those plates are installed tightly with specific screws on the frame equipped with gasket in order to ensure the airtightness of the compartment.

For the present configuration, walls, ceiling and floor consist of two layers, from outside to inside: 2 mm thick steel layer and 25 mm thick calcium silicate layer ( $k = 0.19 \text{ W/m/K}$ ,  $c_p = 960 \text{ J/kg/K}$ ,  $\rho = 770 \text{ kg/m}^3$ ).

At each corner of the floor, cable and pipe clamps are set for measurements and fluids access. The experimental facility is shown in Fig. 1.

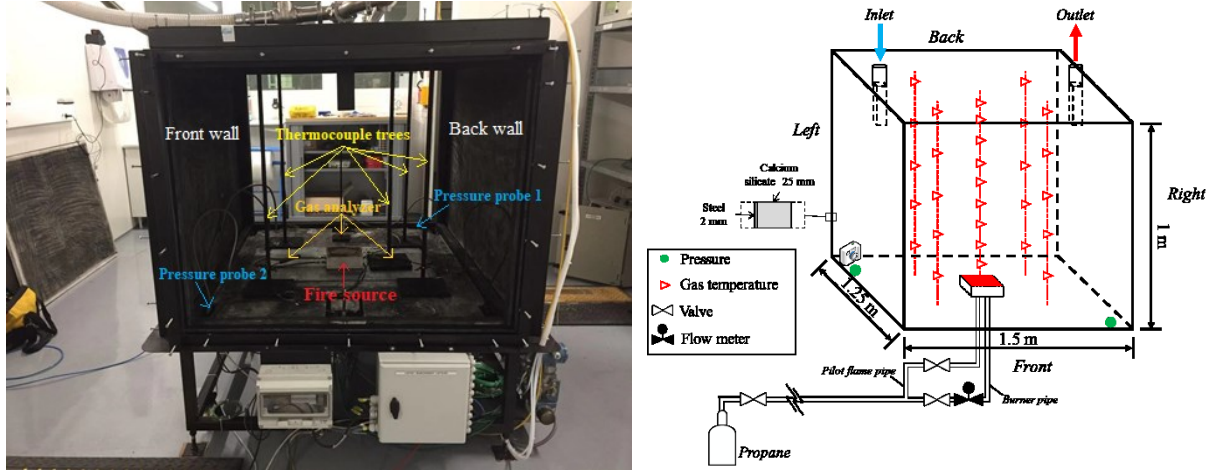


Fig. 1. Experimental facility NYX of IRSN. Left: picture from right view; Right: geometry sketch.

## 2.2. Fire source

The fire source is a square sand propane burner located at the center of the compartment floor and linked to the propane tank through pipes, valves, and a flow meter, as portrayed in Fig. 1. The height and width of the burner are 60 mm and 180 mm, respectively. There is a propane pilot flame, ignited by an electric arc, placed at the edge of the burner. A Bronkhorst mass flow meter/controller is used to impose controllable propane mass flow rates and measure the actually obtained mass flow rates with a range from 0 g/s to 0.4 g/s. The propane flow rate for the pilot flame is not measured. A thermocouple tree is set up to measure the temperatures above the burner, see Fig. 1. More detailed information about the thermocouple tree will be discussed later in section 2.5.

The propane mass flow rate (MFR)  $\dot{m}_f$  (g/s) is prescribed by the controller as follows:

$$\dot{m}_f = \begin{cases} 0 & 0 < t < t_1 \\ \alpha(t - t_1)^n & t_1 < t < t_2 \\ \dot{m}_{f,max} & t_2 < t < t_3 \\ \dot{m}_{f,max} - \alpha(t - t_3)^n & t_3 < t < t_4 \\ 0 & t > t_4 \end{cases} \quad \#(2)$$

In Eq. (2),  $\alpha$  is the flow growth rate ( $\text{g/s}^{n+1}$ ),  $t$  is the time (s),  $n$  is the flow growth exponent (-),  $\dot{m}_{f,max}$  is the maximum propane flow rate (g/s),  $t_1 - t_2$  is the fire growth period (s),  $t_3$  is the time to start decay (s),  $t_4$  is the time when the fire goes out (s). In the present study, two quadratic growth and decay (with an imposed:  $n = 2$ ) are considered with  $\alpha$  of  $3 \times 10^{-5}$  and  $10 \times 10^{-5} \text{ g/s}^3$ . The recorder values of the other parameters are summarized in Table 1. The prescribed propane mass flow rate (MFR) and the experimentally measured MFR are shown in

Fig. 2. The curves align well with each other, although a small jump in the experimental curve is observed at the beginning. This is due to the very small starting flow rate, which is hard to be detected by the meter.

Table 1. Settings for the propane mass flow rate for the different tests.

Config	$\dot{m}_{f,max}$ (g/s)	$\alpha$ (g/s <sup>3</sup> )	$t_1$ (s)	$t_2$ (s)	$t_3$ (s)	$t_4$ (s)
A	0.2	$3 \times 10^{-5}$	60	128	228	308
B	0.1	$1 \times 10^{-4}$	60	84	184	214

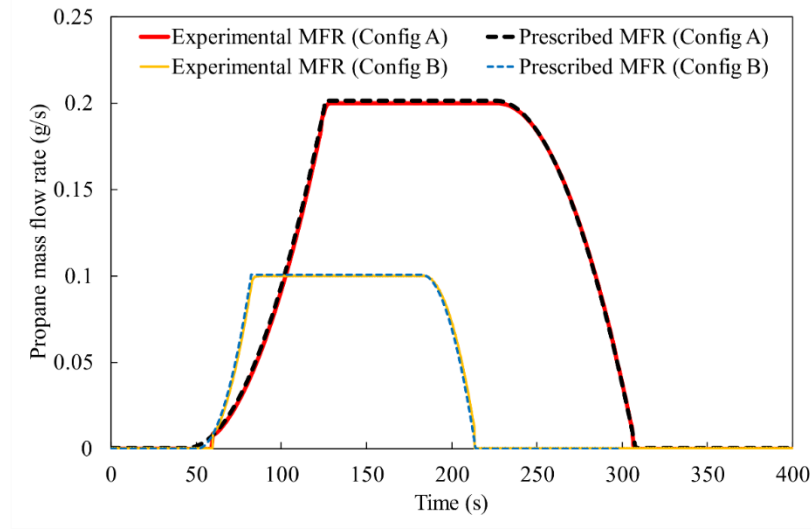


Fig. 2. Experimentally measured and prescribed propane mass flow rates.

### 2.3. Mechanical ventilation system

The mechanical ventilation system consists of admission ducts and extraction ducts, both linked to the ceiling of the compartment, see Fig. 1, and equipped with fans. A sketch of the mechanical ventilation system is shown in Fig. 3. The admission and extraction ducts extend into the compartment through the ceiling for about 21 cm. The duct segments inside the compartment have a rectangular cross section, while the other parts of the ducts have a circular cross section. A 5.6 cm  $\times$  11.9 cm vent is located at each of the rectangular parts for admission and extraction. The admission vent faces the front wall and the extraction vent faces the back wall. When coming out of the compartment, the ducts are linked to a 1.4 m circle metal pipe, where the measuring instruments are installed, lying on the top of the compartment. The admission and extraction flow rates, admission and extraction gas temperatures, extraction gas concentration and extraction pipe pressure are measured in this part. Then, the ducts are connected to a 3 m flexible pipe and 2 m straight pipe leading through the roof of the test room. The diameter of the ducts is 38 mm from the NYX compartment to the test room roof. Above the roof, the ducts are connected to 150 mm diameter pipes. These pipes are bent horizontally and lead to the ventilation fan about 20 m away. After the first bending, there is an electrical valve located in both the admission and extraction ducts. The electrical valves have a variable opening percentage to modify the duct resistance and hence generate different duct flow rates. There are two more bends in the admission duct and one more bend in the extraction duct, which are not shown graphically but indicated in Fig. 3. When reaching the position of the ventilation fan, the ducts

are bent down vertically and connected to the fans. The admission fan sucks fresh air from the experimental hall directly and the extraction fan is linked with an additional duct to release the smoke to the outside. The exhaust fan is equipped with a speed variator whereas the blowing fan has only an On-Off mode. The exhaust fan speed can be adjusted from the control panel by setting a potentiometer in the range of 2.1-5 V.

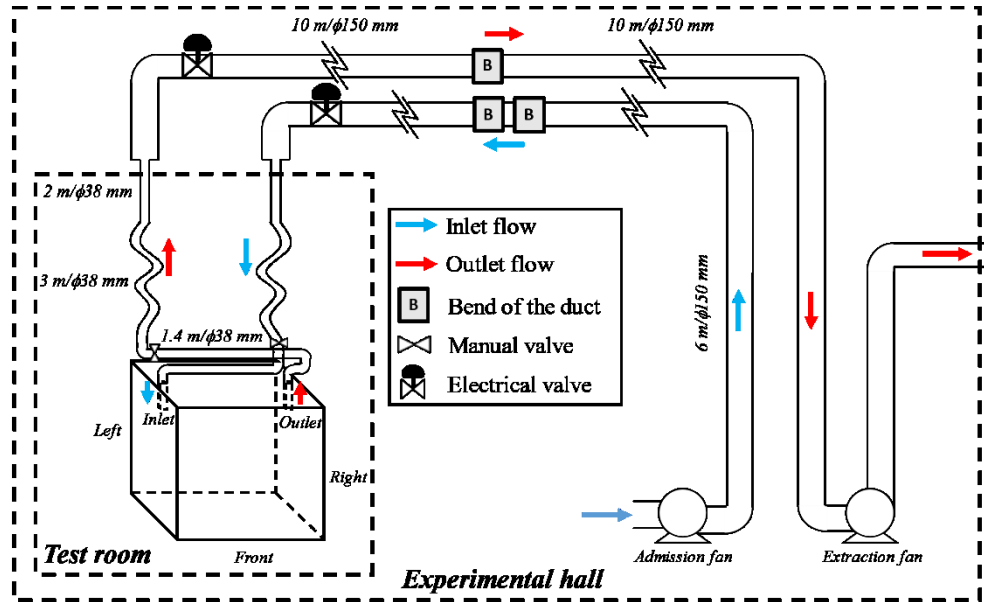


Fig. 3. Sketch of the mechanical ventilation system.

#### 2.4. Test configurations

Cold tests are performed first to evaluate the airtightness of the compartment. Fire tests are then conducted under different ventilation configurations by adjusting the fans' mode (ON/OFF for the admission fan and fan voltage for the exhaust fan) and electrical valves' opening in the ducts to obtain different ventilation resistances and/or different initial ventilation flow rates.

Firstly, for a given fire design (Config A in Table 1), 5 fire tests, (named I to V) are carried out to investigate the influence of ventilation resistances with the same initial ventilation flow rate ( $24 \text{ m}^3/\text{h}$ ). To do so, valves openings, exhaust fan voltage and admission fan activation are set as indicated below:

- Test I: the admission fan is switched off and the duct valves are fully open with the extraction fan voltage set to 3.3 V;
- Test II: the admission fan is switched off, the admission duct valve is fully open and the extraction duct valve is partly open (18 %) with the extraction fan voltage set to 4 V;
- Test III: the admission fan is switched off, the admission duct valve is fully open and the extraction duct valve is partly open (16.9 %) with the extraction fan voltage set to 4.8 V;
- Test IV: the admission fan is switched on, the admission duct valve is partly open (25 %) and the extraction duct valve is fully open with the extraction fan voltage set to 3.3 V;
- Test V: the admission fan is switched on, the admission duct valve is partly open (24 %) and the extraction duct valve is partly open (18 %) with the extraction fan voltage set to 4.5 V.

The influence of the initial ventilation flow rate on the fire dynamics are investigated with 3 tests (named VI to VIII) with a second fire design (Config B in Table 1). For this set of tests, the admission fan is switched off and the duct valves are fully open with a given extraction fan voltage:

- Test VI: the extraction fan voltage set to 2.7 V;
- Test VII: the extraction fan voltage set to 3.3 V;
- Test VIII: the extraction fan voltage set to 4.1 V.

A higher extraction fan voltage leads to a higher fan speed. The tested configurations are summarized in Table 2. The acronym as used in the test campaign is added to the table for future referencing.

Table 2. Summary of the test settings. AF: admission fan. AV: valve in the admission duct. EV: valve in the extraction duct. EF: voltage imposed on the extraction fan. Positions of the fans and valves are shown in Fig. 6.

Test	HRR config	Name in the test campaign	AF	AV	EV	EF (V)	Initial flow rate (m <sup>3</sup> /h)
I	A	F1AA2	OFF	Fully open	Fully open	3.3	24
II	A	VCA1	OFF	Fully open	Partly open	4	24
III	A	VCA2	OFF	Fully open	Partly open	4.8	24
IV	A	VCB1	ON	Partly open	Fully open	3.3	24
V	A	VCC1	ON	Partly open	Partly open	4.5	24
VI	B	VCA3a	OFF	Fully open	Fully open	2.7	12
VII	B	VCA4a	OFF	Fully open	Fully open	3.3	24
VIII	B	VCA6	OFF	Fully open	Fully open	4.1	40

## 2.5. Measurements

The gauge pressure, gas temperature, and ventilation flow rates are recorded during the experiments. Two pressure tubes and five thermocouple trees are placed inside the compartment. The positions of the instruments in the compartment are depicted in Fig. 4. Thermocouples, Pitot probes, and pressure tube are placed in the ventilation ducts lay on the top of the compartment, see Fig. 5. The original parameters measured directly and the calculated parameters are listed in Table 3.

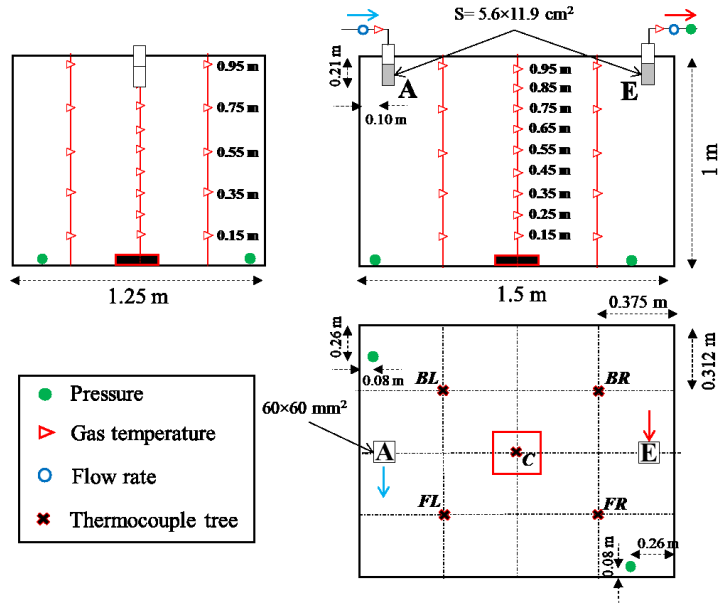


Fig. 4. Measurements inside the compartment. Top-left: left view; Top-right: front view; Bottom-right: top view.

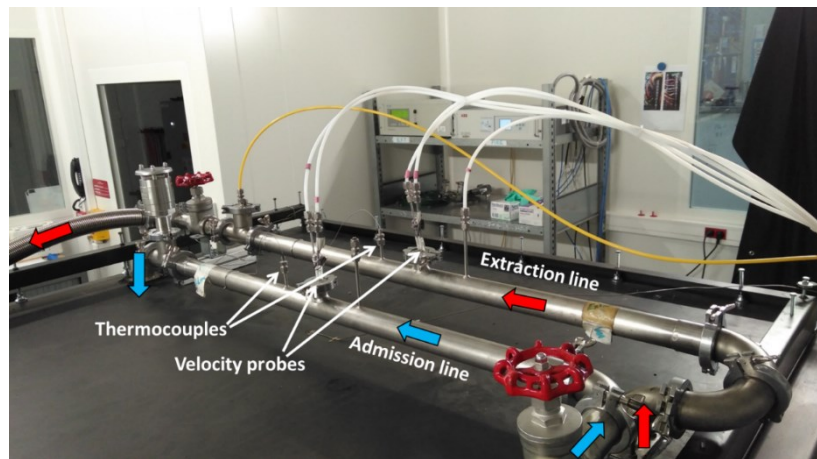


Fig. 5. Measuring points in the ventilation ducts on the top of the compartment.

Table 3. Measured parameters and calculated parameters. Ticked boxes indicate the measured parameters used to obtain the calculated parameters.

Instrument	Measured parameter	Calculated parameter	
		Flow resistance	Mass capacity
Pressure transducer	Gauge pressure	✓	
Pitot probe	Duct volume flow rate	✓	
Thermocouple	Temperature		✓
Flow meter	Propane mass flow rate		

### 2.5.1. Pressure

The pressure tube is linked to one connector of the pressure transducer (Rosemount 3051), and the other connector is open to the environment. Therefore, the pressure difference between the measuring point and the environment, i.e., the relative pressure, is recorded. The locations of the pressure measuring points in the compartment are indicated in Fig. 4. Along the ventilation ducts, pressures are also recorded at several points to calculate the duct resistance, as sketched in Fig. 6 (green dots). For the fan pressure measurements, the pressure transducer connectors are linked via tubes to the upstream and downstream of the fans.

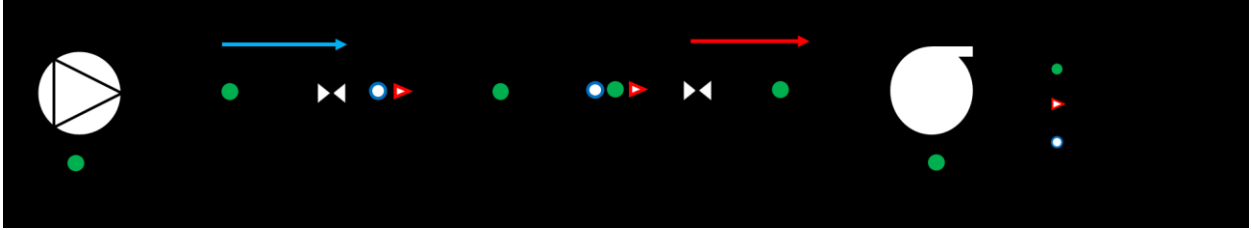


Fig. 6. Pressure measurement points (green dots) in the mechanical ventilation system. Note that the schematic just indicates the relative position of the measurements, not refer to the actual scale. AV: electrical valve in the admission duct. EV: electrical valve in the extraction duct.  $\Delta p$ : gauge pressure (Pa) in the NYX compartment.

### 2.5.2. Flow resistance

The resistance of the ventilation duct is calculated based on the pressure difference between the upstream and downstream of the ducts and the duct volume flow rate:

$$\Delta p_{resis} = \frac{1}{2} r' \rho v^2 = \frac{1}{2} r' \rho \left( \frac{\dot{q}}{A} \right)^2 \quad \#(3)$$

$$r' = \frac{2 \Delta p_{resis}}{\rho} \cdot \left( \frac{A}{\dot{q}} \right)^2 \quad \#(4)$$

where  $\Delta p_{resis}$  is the pressure drop due to the duct resistance (Pa),  $r'$  is the dimensionless resistance of the duct (-),  $\rho$  is the fluid density ( $\text{kg/m}^3$ ),  $v$  is the flow velocity (m/s),  $\dot{q}$  is the duct volume flow rate ( $\text{m}^3/\text{s}$ ),  $A$  is the duct area ( $\text{m}^2$ ). As described in section 2.3, the ventilation ducts' cross-sectional areas are not constant. In order to easily determine the resistance by experiments, a resistance factor  $r''$  in  $\text{m}^{-4}$  can be considered to avoid counting the area:

$$r'' = \frac{r'}{A^2} = \frac{2 \Delta p_{resis}}{\rho \cdot \dot{q}^2} \quad \#(5)$$

This resistance factor can be determined for the admission duct ( $r''_{adm}$ ) and the extraction duct ( $r''_{ext}$ ) separately. In case of reverse flow in either of the ducts, the extraction/supply of gases from/into the compartment occurs through the ducts in parallel and the equivalent network flow resistance ( $r''_{eq}$ ) can be defined as [3]:

$$r''_{eq} = \left( \frac{1}{r''_{adm}} + \frac{1}{r''_{ext}} \right)^{-1} \quad \#(6)$$

The calculation uses the data acquired prior to ignition. The admission and extraction duct resistances for the tested cases are calculated using Eq. (5), using  $\Delta p_{AF} - \Delta p$  and  $\Delta p + \Delta p_{EF}$ , where  $\Delta p$  is the gauge pressure (Pa) in the NYX compartment,  $\Delta p_{AF}$  and  $\Delta p_{EF}$  are recorded as the local pressure difference in Pa over the admission fan (AF) and the extraction fan (EF), respectively (see Fig. 6). The pressure differences are defined as downstream pressure minus upstream pressure (i.e.,  $\Delta p_{AF} > 0$  and  $\Delta p_{EF} > 0$ ). Note that this calculation implies that the upstream side of the admission fan and the downstream side of the extraction fan are directly connected to the ambient. In the set-up at hand this is the case for the admission fan but not really for the extraction fan, which is connected to the ambient through an additional duct, as described in section 2.3. However, this additional duct is short compared to the other ventilation branches, so the pressure drop along this duct is not considered here. The obtained admission (adm) and extraction (ext) resistances of the tests are listed in Table 4. They are computed from the initial flow rate conditions prior to ignition (with subscript 'init'). It can be seen that the duct resistance factor  $r''$  varies with different valve opening (see section 2.4) for tests I-V. Test I is the least resistive configuration, whereas test V is the most resistive one. For tests VI-VIII, the resistance factors  $r''$  of the duct are similar and small, because the valves are all fully open; only the initial ventilation flow rate varies. The slight deviations in the resistance factor when the valves are fully open might be caused by the mechanical error of the valve control.

The configuration can also be examined through an analogy with electrical network (see appendix). From that analogy, the following quantities appear, also included in Table 4:

$$R_{flow} = \frac{\Delta p_{resis}}{\dot{m}} = \frac{r' \cdot v}{2A} = \frac{r'' \cdot \dot{q}}{2} \#(7)$$

where  $R_{flow}$  is the electrical analogy equivalent flow resistance ( $\text{m}^{-1} \cdot \text{s}^{-1}$ ),  $\dot{m}$  is the mass flow rate in the duct (kg/s). The network total equivalent flow resistance is then defined as:

$$R_{eq} = \left( \frac{1}{R_{flow,adm}} + \frac{1}{R_{flow,ext}} + \frac{1}{R_{flow,leak}} \right)^{-1} \#(8)$$

As the leakage flow resistance is normally much higher than the mechanical ventilation flow resistance, the term  $1/R_{flow,leak}$  is considered negligible. This is then very similar to Eq. (6).

It is worth noting that the flow resistance in Eq. (7) changes with the flow rate whereas the dimensionless resistance  $r'$  and the resistance factor  $r''$  do not, as they only depend on the duct dimensions and geometry.

Table 4. Ventilation resistances and time scales for different tests prior to ignition.

Parameter	Test I	Test II	Test III	Test IV	Test V	Test VI	Test VII	Test VIII
$r''_{adm} (\times 10^6 \text{ m}^{-4})$	3.27	3.32	3.30	66.9	65.8	4.16	3.27	2.93
$r''_{ext} (\times 10^6 \text{ m}^{-4})$	4.92	19.3	36.0	5.06	28.6	4.35	4.94	4.96
$r''_{eq} (\times 10^6 \text{ m}^{-4})$	1.96	2.83	3.02	4.70	19.9	2.13	1.97	1.84
$R_{flow,admit} (\times 10^4 \text{ m}^{-1} \text{ s}^{-1})$	1.06	1.03	1.09	21.8	21.5	0.69	1.08	1.62
$R_{flow,extinit} (\times 10^4 \text{ m}^{-1} \text{ s}^{-1})$	1.70	6.29	12.5	1.72	9.87	0.75	1.71	2.88

$R_{eq,mit}$ ( $\times 10^4$ m <sup>-1</sup> s <sup>-1</sup> )	0.65	0.89	1.00	1.60	6.77	0.36	0.66	1.04
--	------	------	------	------	------	------	------	------

### 2.5.3. Ventilation flow rate

The ventilation flow rates are measured using the bi-directional velocity Pitot probe technique. The probe is positioned at the center of the duct section and connected to pressure transducers where the pressure difference induced by flow speed is measured. The volumetric flow rate can be calculated from:

$$\dot{q} = 3600 \times k(\Delta p_{flow}) A \sqrt{\frac{2\Delta p_{flow}}{\rho}} \quad \#(9)$$

where  $\dot{q}$  is the volumetric flow rate (m<sup>3</sup>/h),  $k$  is the calibration factor varying with the pressure,  $A$  is the duct area (m<sup>2</sup>),  $\Delta p_{flow}$  is the pressure difference (Pa) induced by flow speed and  $\rho$  is the gas density (kg/m<sup>3</sup>).

The calibration factor is determined before the tests by comparing the measured flow rate with a reference flow rate given by another measurement apparatus (pipe equipped with orifice plate) inserted on each line. The calibration factor varies with the pressure difference as well as the direction of the flow. The calibration results are shown in Fig. 7. Relations indicated in Fig. 7 are introduced in the acquisition system.

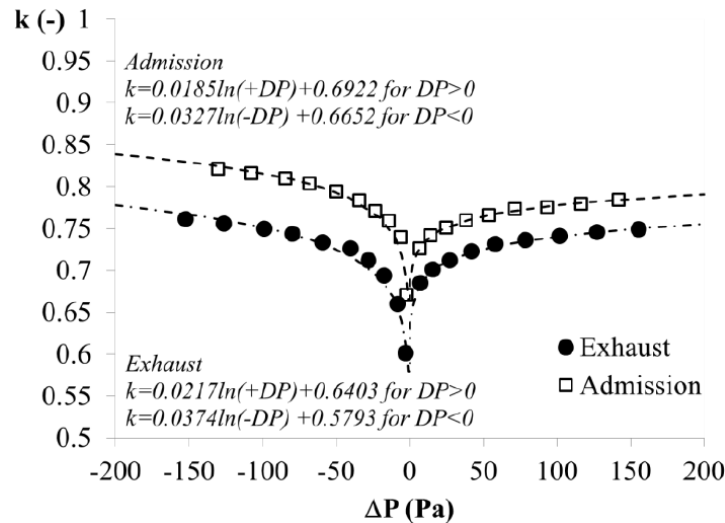


Fig. 7. Calibration factor versus the pressure difference for the two ventilation lines.

The acquisition of the data and the control of the facility are performed with two cDAQ - 9189 CompactDAQ Ethernet chassis designed for small, distributed sensor measurement systems. Each chassis controls the timing, synchronization, and data transfer between C Series I/O modules and an external host.

### 2.5.4. Temperature

The thermocouple tree at the center (labeled as C in Fig. 4) of the compartment has nine K-type 0.5 mm bead diameter thermocouples from 0.15 m to 0.95 m from the floor, with a distance of 0.1 m from each other. The other four surrounding thermocouple trees in Fig. 4, namely FL

(Front-Left), FR (Front-Right), BL (Back-Left) and BR (Back-Right), have five K-type 0.5 mm bead diameter thermocouples from 0.15 m to 0.95 m from the floor, with a distance of 0.2 m from each other. There are also 1.5 mm bead diameter K-type thermocouples placed on the middle of the outside surface of the top, front, back and left walls. Besides, there is a 0.5 mm bead diameter K-type thermocouple placed at the vicinity of the pilot flame. Moreover, the gas temperatures are measured in the admission and extraction ducts near the compartment using 0.5 mm bead diameter K-type thermocouples. On top of this, the gas temperature is also measured with a 1.5 mm bead diameter K-type thermocouple located in the ventilation network close to the extraction fan.

## 2.6. Experimental uncertainty

The testing ranges and uncertainties of the measurement apparatuses are estimated and listed in Table 5. The uncertainties are evaluated by performing calibration tests using the data provided by the manufacturers. Some tests are repeated several times to assess to test repeatability which is confirmed to be good by the results. The standard uncertainties are obtained under conditions without fire. Therefore, a coverage factor is introduced to take into account the influence of fire on the standard uncertainty. Thus, the uncertainty of measurements with fire is the standard uncertainty multiplied by the coverage factor [3].

Table 5. List of measuring ranges and uncertainties.

Variable	Range	Standard uncertainty	Coverage factor
Pressure	[0-5000] Pa	0.1 %FS	2
Gas temperature	[0-1300] K	2 °C	2 (5 for flame temperature)
Gas flow rate	[0-60] m <sup>3</sup> /h	0.1%RD+0.3%FS	2
Propane flow rate	[0-4] g/s	0.5%RD+0.1%FS	2

*FS= Full scale; RD= Reading data*

## 2.7. Airtightness estimation

Apart from the mechanical ventilation system, it is noted that the leakage flow also contributes to the ventilation of the compartment to some extent. However, the leakage flow might be less important compared to the mechanical ventilation flows in a mechanically-ventilated air-tight compartment. Besides, the leakage flow rate can be used to evaluate the airtightness of the compartment, i.e., lower leakage flow corresponds to better airtightness. The airtightness (leakage flow rate) of the NYX facility is estimated experimentally by a leakage flow test: 1) pressurize (depressurize) the compartment to a certain level of pressure, 2) let the pressure recover to the initial level through leaking, see Fig. 8. Three leakage flow tests were conducted, namely before the fire test series (Leak test A), during the fire test series (Leak test B), and after completion of the fire test series (Leak test C). The leakage flow rate is calculated based on mass conservation of gas within the compartment with closed admission and exhaust line and the ideal gas law. The mass conservation tells that the time derivative of mass is equal to the leakage mass flow rate:

$$\frac{dm}{dt} = \dot{m}_L \Rightarrow V \frac{d\rho}{dt} = \rho \dot{q}_L \#(10)$$

The gas density can be obtained from the ideal gas law:

$$\rho = \frac{PM}{rT} \#(11)$$

Combining Equations (10) and (11), the following expressions can be obtained:

$$\frac{VM}{rT} \frac{dP}{dt} = \frac{PM}{rT} \cdot \dot{q}_L \#(12)$$

$$\dot{q}_L = \frac{V}{P} \cdot \frac{dP}{dt} \#(13)$$

where  $P$  is the absolute pressure inside the compartment (Pa),  $V$  is the volume of the compartment ( $\text{m}^3$ ),  $r$  is the ideal gas constant ( $8.314 \text{ J}/(\text{mol}\cdot\text{K})$ ),  $T$  is the absolute temperature of the gas (K),  $m$  is the mass of gas inside the compartment (kg),  $M$  is the gas molar mass ( $\text{kg}/\text{mol}$ ),  $t$  is time (s),  $\dot{m}_L$  is the leakage mass flow rate ( $\text{kg}/\text{s}$ ),  $\rho$  is gas density ( $\text{kg}/\text{m}^3$ ),  $\dot{q}_L$  is the leakage volume flow rate ( $\text{m}^3/\text{s}$ ).

Fig. 8 shows the pressure recovery curves after pressurizing and depressurizing for three set of tests (A, B and C) performed during the test campaign. The leakage flow rate increases linearly with higher pressure difference between indoor and outdoor, as can be seen in Fig. 9. Clear differences can be observed between the leakage tests. The leakage flow rate is the highest before the fire test series and the lowest after the fire test series. It is conjectured that the fire-induced fumes and soot may accumulate in the gaps, cracks or joints, which leads to the decrease of leakage. A zoom-in of the curves around the coordinate origin shows a slight shift of curves. This is due to the sampling operation of the gas analyzer to suck gas at a constant rate. Therefore, the pressure is negative at the initial state. It is noted that the pressures also recover to a negative value in Fig. 8. The gas analyzer extraction rate is about 1 L/min (i.e.,  $0.06 \text{ m}^3/\text{h}$ ), which corresponds to the intercept in Fig. 9.

The air change rate at a certain pressure, e.g., 50 Pa [19], can be used to evaluate the airtightness:

$$n_{50} = \frac{\dot{q}_{L,50}}{V} \#(14)$$

where  $n_{50}$  is the air change rate (1/h) at a pressure difference of 50 Pa,  $\dot{q}_{L,50}$  is the leakage flow rate ( $\text{m}^3/\text{h}$ ) at a pressure difference of 50 Pa,  $V$  is the volume of the compartment ( $\text{m}^3$ ). Hence, the air change rate at a pressure difference of 50 Pa calculated according to the leakage tests A, B and C are 0.13 1/h, 0.08 1/h and 0.06 1/h, respectively. For the passive houses, which represent high air-tight level residential buildings, the air change rate at 50 Pa should be lower than 0.6 1/h [16]. This illustrates that the NYX compartment has a high level of airtightness. An example of the calculation of  $R_{flow,leak}$  at a pressure difference of 50 Pa using Eqs. (5) and (7) gives an equivalent resistance of leakage to be  $6.2 \times 10^5 \text{ m}^{-1}\cdot\text{s}^{-1}$ , which is much higher than most of the duct resistances in Table 4. Hence, in the determination of the equivalent resistance (Eqs. (6) and (8)), the contribution of the leakage is negligible.

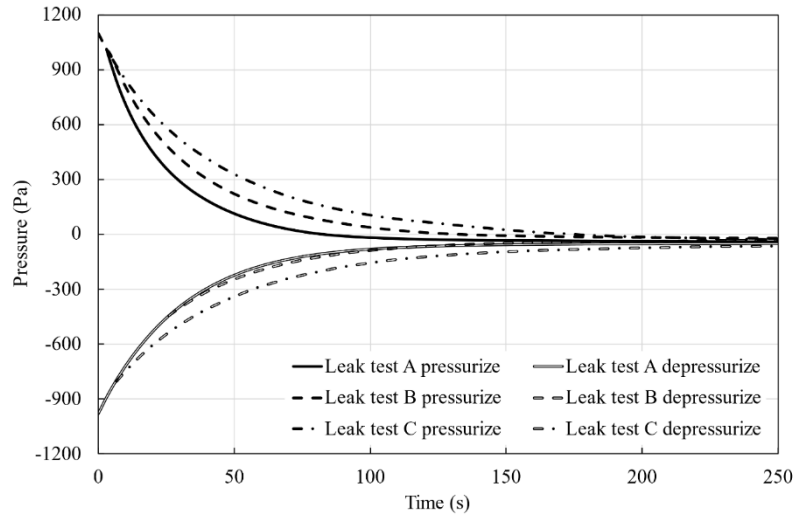


Fig. 8. Pressure recovery curves after pressurizing and depressurizing for three sets of tests (A, B and C) performed during the test campaign.

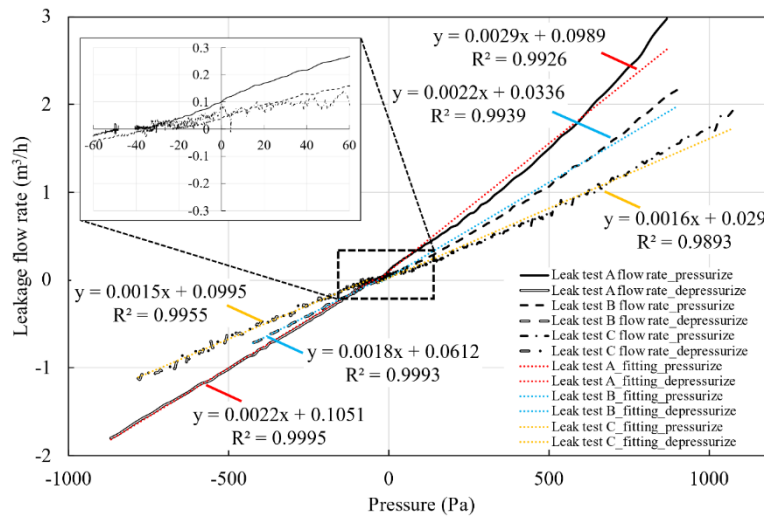


Fig. 9. Leakage flow rate as function of pressure difference between indoor and outdoor. A: before the fire tests. B: during the fire test series. C: after completion of the fire test series.

### 3. Results and discussion

#### 3.1. General temporal profiles of the pressure

The overall pressure evolution inside the compartment is shown in Fig. 10 for test I. It follows the imposed propane mass flow rate evolution during the growth and decay phase, and relaxes towards steady values during phases of steady propane mass flow rate. The different stages are indicated by shadows. The pre-ignition stage is included to record the steady operating ventilation conditions without fire. Due to the extraction flow at this stage, the initial pressure is negative. In the growth phase, the pressure rise has a slight delay compared to the rise of propane mass flow rate at first. The first reason is that the propane flow rate was very low at the beginning, which caused some accumulation of fuel before the pilot flame could ignite the propane. Secondly, because the propane flow rate is measured about one meter upstream the

burner, it takes some time for the propane to flow from the measuring point to the burner. However, with the speed-up of the propane flow rate, this time becomes negligible. During the fire growth stage, the pressure rises continuously until the propane mass flow rate reaches the maximum value, see Fig. 10. Then, the pressure starts decreasing to a quasi-steady value while the propane flow rate kept at its maximum. When the fire (and the propane flow rate) starts decreasing, the pressure follows and drops to an under-pressure lower than the initial pressure. After the fire extinguishment (propane flow rate null), the pressure goes back towards the initial level gradually.

From a qualitative point of view, the pressure evolution is similar for all tests. However, the magnitudes of pressure vary significantly, as discussed in section 3.3.

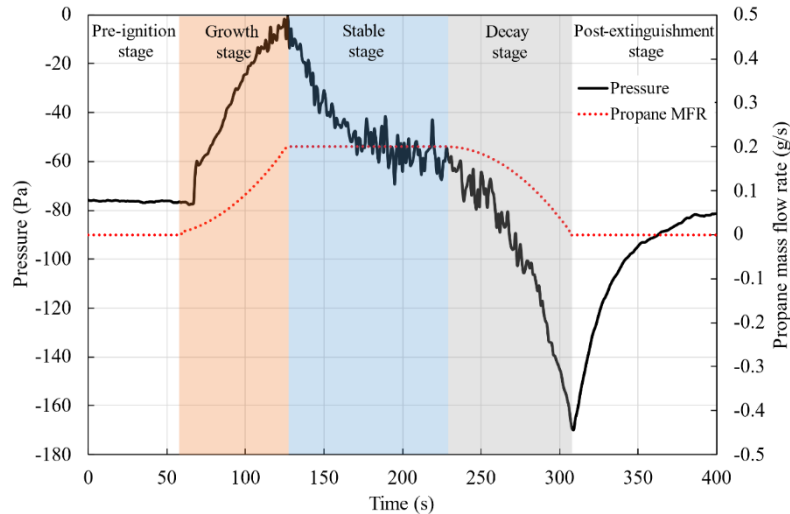


Fig. 10. Pressure and propane mass flow rate (MFR) evolutions as function of time in Test I.

### 3.2. Temporal evolutions of the ventilation flow rate

As mentioned, the present study focuses on the impact of the ventilation settings on the fire dynamics, and in particular on the pressure, inside the compartment. Hence, it is important to discuss the evolution of the ventilation flow rates.

From Fig. 10, it is clear that there will first be an increase in pressure inside the compartment during the growth phase. This will counter-act the admission of fresh air and enhance the extraction of gases from the compartment. The opposite occurs during the strong under-pressure period during the decay phase of the fire.

The qualitative pressure lines sketched in Fig. 11 for the two situations with the admission fan turned off and on, illustrate the effect on the ventilation flow rate. Prior to the ignition of the fire, the air flows from ambient to the compartment through admission ducts and goes out to the ambient via extraction ducts. If the admission fan is turned on, there will be a pressure increase induced by the admission fan, as shown in Fig. 11 (b). Then, the pressure will drop along the ducts because of the resistance. Finally, the extraction fan will raise the pressure to the ambient level. The qualitative influence of fire-induced pressure on the ventilation flow rates is depicted in Fig. 11.

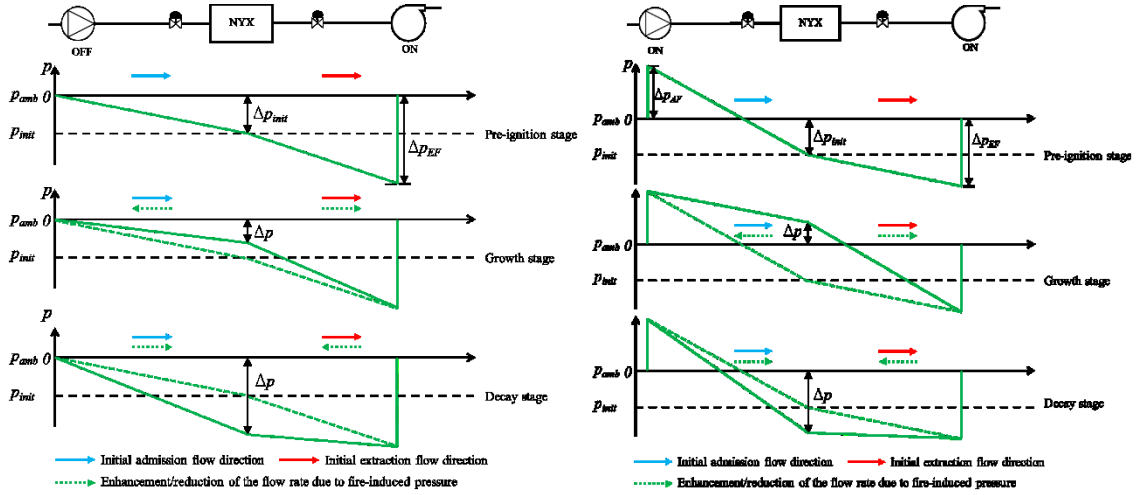


Fig. 11. Schematic diagram showing qualitative pressure changes along the ventilation ducts before fire and during fire when the admission fan is turned off (left) and on (right).

It is now important to assess this in quantitative terms. The impact of the pressure inside the compartment on the admission and extraction flow rates will depend on the flow resistances. This can be understood from Eq. (5) recall here in a general form:

$$\dot{q} = \sqrt{\frac{2\Delta p_{resis}}{r'' \cdot \rho}} \#(15)$$

Here,  $\Delta p_{resis}$  is the pressure difference (Pa) between 2 points in the ventilation system and  $\rho$  is the fluid density ( $\text{kg/m}^3$ ), depending on the fluid temperature. The fire-induced pressure will now modify  $\Delta p_{resis}$  from the initial value ( $\Delta p_{resis,init}$ ) to the new value. In the growth phase,  $\Delta p_{resis} < \Delta p_{resis,init}$  in the admission duct, while the opposite is true in the extraction duct. Assuming the resistance factor ( $r''$ ) is a constant, the ratio between the modified flow rate (due to the fire-induced pressure evolution) and the initial flow rate reads:

$$\frac{\dot{q}}{\dot{q}_{init}} = \sqrt{\frac{\Delta p_{resis}}{\Delta p_{resis,init}}} \cdot \sqrt{\frac{\rho_{init}}{\rho}} \#(16)$$

Let us now consider the pressure inside the compartment, compared to the pressure level inside the compartment prior to ignition  $\Delta p - \Delta p_{init}$ . Then, in the growth phase  $\Delta p - \Delta p_{init} > 0$  and two situations should be addressed for the admission duct:

$\Delta p_{AF} - \Delta p \geq 0$  : no reverse flow in the admission duct;

$\Delta p_{AF} - \Delta p < 0$  : reverse flow in the admission duct.

This then leads to the following:

$$\dot{q}_{adm} = \begin{cases} \dot{q}_{adm,init} \cdot \sqrt{1 - \frac{\Delta p - \Delta p_{init}}{\Delta p_{AF} - \Delta p_{init}}} (\Delta p_{AF} \geq \Delta p) \\ \dot{q}_{adm,init} \cdot \sqrt{\frac{\Delta p - \Delta p_{init}}{\Delta p_{AF} - \Delta p_{init}}} - 1 \cdot \sqrt{\frac{\rho_{adm,init}}{\rho_{adm}}} (\Delta p_{AF} < \Delta p) \end{cases} \quad \#(17)$$

For the extraction flow rate, there is no possibility for reverse flow in the growth phase since the pressure increases:

$$\dot{q}_{ext} = \dot{q}_{ext,init} \cdot \sqrt{1 + \frac{\Delta p - \Delta p_{init}}{\Delta p_{EF} + \Delta p_{init}}} \cdot \sqrt{\frac{\rho_{ext,init}}{\rho_{ext}}} \quad \#(18)$$

The same reasoning holds for the decay phase, but now  $\Delta p - \Delta p_{init} < 0$  and there might be reverse flow in the extraction duct. The densities are calculated by virtue of the ideal gas law and using the temperature measurements at the admission and extraction ducts.

It is key to note now that for a given flow rate ( $\dot{q}_{init}$ ) before the change in the fire HRR (rise or decay), the pressure drop  $\Delta p_{resis,init}$  is larger for higher resistance (Eq. (15)). This implies that the impact of a fire-induced variation of pressure inside the compartment on the admission and extraction flow rates is smaller as the flow resistance is larger. This is true when the equivalent network resistance is used (i.e., when considering the flow resistance globally), but it also applies to the flow through the admission and extraction ducts separately, as discussed next.

Compare first test I with tests II and III in Fig. 12. The flow resistance in the admission duct remains unchanged (Table 4) while the flow resistance in the extraction duct is higher for tests II and III. It is clearly seen that the flow rate varies less in the extraction duct and more in the admission duct for tests II and III, compared to test I. Tests II and III nearly reach the condition of reverse flow at admission. In test IV, the resistance in the admission duct is much higher than for the tests I to III and this leads to very little variation in the admission flow rate, compared to the extraction flow rate, as expected. Finally, test V confirms that increasing both flow resistances leads to more comparable variations in admission and extraction flow rates, and that these variations are relatively small. These results illustrate the change of flow rate in case of pressure variation and the influence of the flow resistances on the amplitude of these flow rate variations. It is also proven that not only the total, or 'equivalent', flow resistance is important, but also the flow resistances in the admission and extraction ducts separately (or, equivalently, the ratio of the individual admission and extraction flow resistance).

Fig. 13 shows the results for tests VI-VIII. As the flow resistance ( $r''$ ) is small and nearly identical (Table 4) in both admission and extraction duct, the variation in flow rate is quite significant. The change in the initial flow rate does not modify the amplitude of variation of flow rate during the combustion phase: they are nearly the same for the three tests, because the flow resistances are identical. For test VI, the low flow rate prior to ignition (about 12 m<sup>3</sup>/h) leads to a period of reversed flow in the admission duct between 80 s and 100 s. It is also noted that the admission and extraction flow rates are not identical prior to the fire in Fig. 12 and Fig. 13. Firstly, these discrepancies are within the measurement uncertainties. Besides, the initial negative pressure leads to inward leakage flows, resulting in a slightly higher extraction flow rate compared to the admission flow rate, which is the case shown in Fig. 12 and Fig. 13.

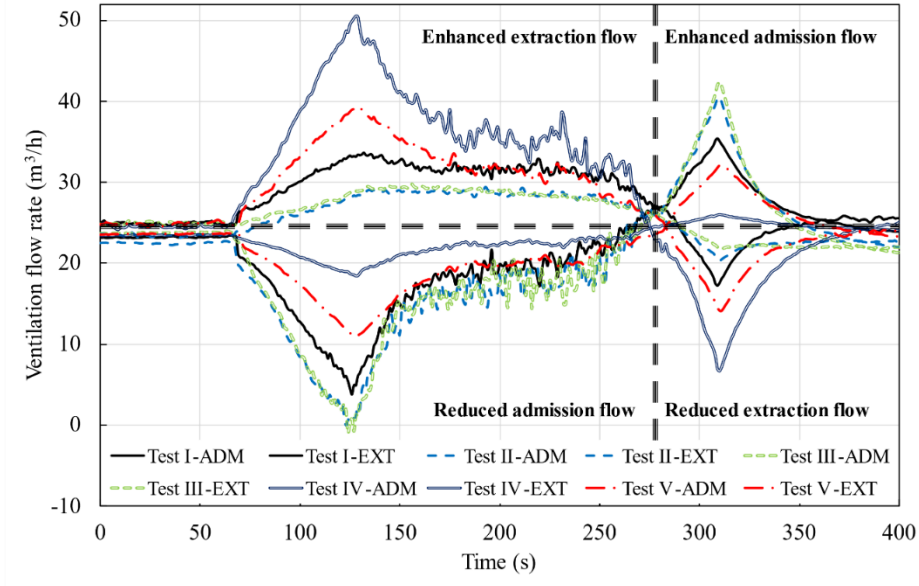


Fig. 12. Ventilation flow rates as function of time for tests I-V with various air flow resistances and identical ventilation flow rate before ignition. Top-left quadrant: enhanced extraction flow; Bottom-right quadrant: reduced extraction flow; Bottom-left quadrant: reduced admission flow; Top-right quadrant: enhanced admission flow. Test I:  $r''_{adm}/r''_{ext} = 0.66$ ; Test II:  $r''_{adm}/r''_{ext} = 0.17$ ; Test III:  $r''_{adm}/r''_{ext} = 0.09$ ; Test IV:  $r''_{adm}/r''_{ext} = 13.22$ ; Test V:  $r''_{adm}/r''_{ext} = 2.3$ .

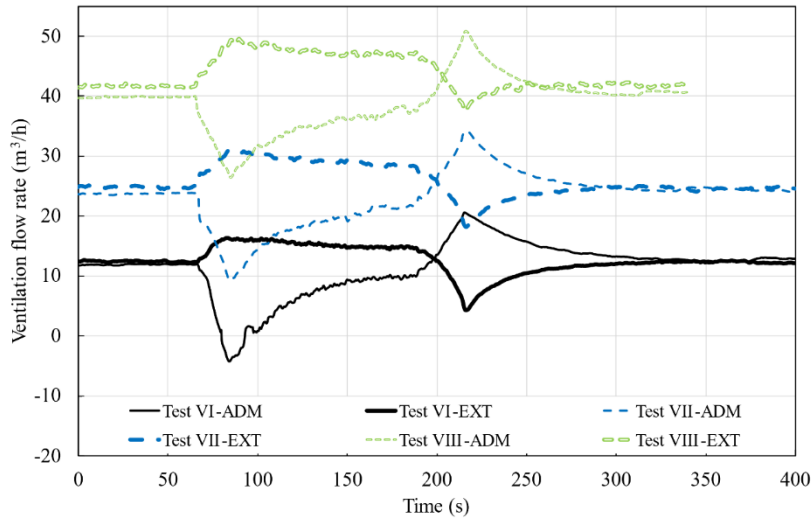


Fig. 13. Ventilation flow rates as function of time for tests VI-VIII with similar flow resistance factors in both lines but various initial ventilation flow rate.

### 3.3. Influence of the ventilation settings on the pressure

The influence of the ventilation configurations on the pressure variation is evaluated by varying the duct resistance ( $r''$ ) or changing the initial ventilation flow rate ( $\dot{q}_{init}$ ). In fact, these variations can be reflected in  $R_{eq}$  (Eq. (8)) or  $r''_{eq}$  (Eq. (6)). The details are discussed hereafter in separate subsections.

### 3.3.1. Influence of the flow resistance

Consider first tests I, II and III (Fig. 14). The flow resistance in the admission duct is unchanged, but the flow resistance in the extraction duct increases from test I to III. In order to have the same initial air flow rate (Fig. 12), a higher voltage is applied to the extraction fan (the pressure difference at the fan,  $\Delta p_{EF}$  increases). In the growth phase, the pressure evolution is very similar in all 3 tests. Starting from ambient, the temperature (thermal effect) is lower in the growth phase than in the decay phase. This results in the similar over-pressures in tests I-III. Besides, in tests II and III, the extraction flow resistances ( $R_{ext}$ ) are higher when the extraction fan pressure ( $\Delta p_{EF}$ ) increases, which results in the extraction flow rates enhanced less and the admission flow rates reduced more in tests II and III. Hence, similar pressure variations as test I are obtained. Subsequently, the pressure relaxes to a steady value, until the decay phase starts. Now the main aspects in Eq. (1) are the reduction in fire HRR, as well as the heat losses through the extraction duct and walls. Whereas the fire HRR evolution is identical in all 3 tests during the decay phase, the extraction flow rate is significantly more reduced in test I, compared to test II and test III (Fig. 12). The latter has the least reduction in extraction flow rate. Hence, the pressure drop is the strongest in test III, and the least in test I. This clearly illustrates the importance of not only the total flow resistance, but also the flow resistance in the admission and extraction duct separately.

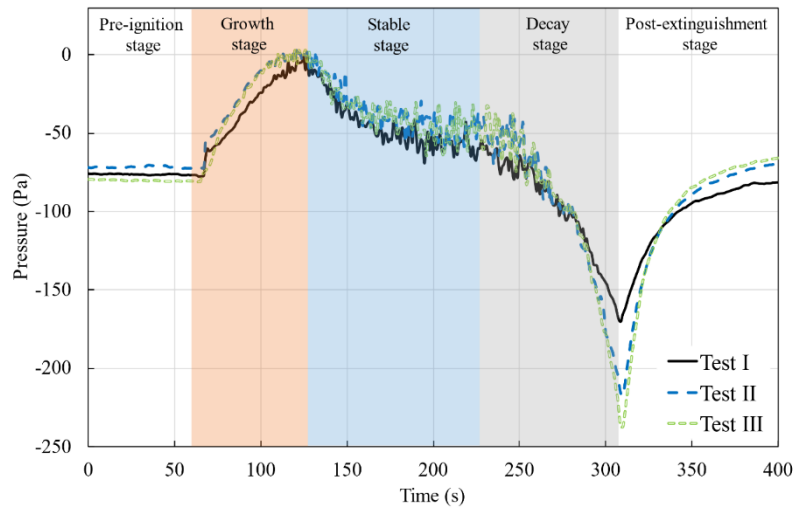


Fig. 14. Pressure variations for the tests with the admission fan switched off. Test I:  $r''_{eq} = 1.96 \times 10^6$ ,  $R_{eq,init} = 6.5 \times 10^3$ ; Test II:  $r''_{eq} = 2.83 \times 10^6$ ,  $R_{eq,init} = 8.9 \times 10^3$ ; Test III:  $r''_{eq} = 3.02 \times 10^6$ ,  $R_{eq,init} = 1.0 \times 10^4$ .

Consider now test V (Fig. 15), compared to test I. In both cases the flow resistances at admission and extraction ducts are of the same order of magnitude, but the total resistances are much higher in test V ( $r''_{eq} \sim 20 \times 10^6 \text{ m}^{-4}$ ) than in test I ( $r''_{eq} \sim 2 \times 10^6 \text{ m}^{-4}$ ). It can be seen that both the over-pressure and under-pressure are much stronger in test V than in test I. This clearly illustrates that a higher total, or ‘equivalent’, flow resistance leads to much more pronounced fire-induced pressure peaks (positive and negative), see Fig. 16. The initial ventilation flow rates are identical in tests I-V, so the plots in Fig. 16 with  $r''_{eq}$  and  $R_{eq,init}$  give the same trends, see Eq. (7).

Note that the crossing lines in Fig. 16 indicate that the over-pressure peak is lower than the under-pressure peak in tests I-III, whereas for tests IV and V it is the opposite. The over-pressure peak means the pressure difference between the peak value at the end of the growth stage, compared to the initial pressure. The under-pressure peak refers to the pressure difference between the minimum value at the end of the decay stage and the quasi-steady pressure value during the stable period ahead of the decay phase. The pressure evolution along the ventilation system shown in Fig. 17 indicates that the fan operation in tests IV and V changes the pressure line shape significantly. For all the other cases, the extraction fan ( $\Delta p_{EF}$ ) is always on, while the admission fan is off, leading to  $\Delta p_{over} < \Delta p_{under}$ . In the current tests, the admission fan is much stronger than the extraction fan, and thus the fan operation is considered to be the primary effect resulting in the occurrence of the crossing lines.

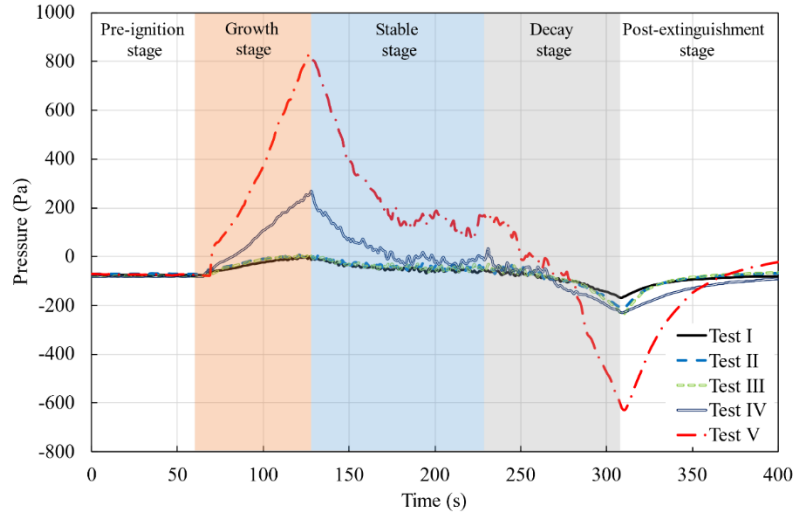


Fig. 15. Pressure variations as function of time in tests with different ventilation resistance. Test I:  $r''_{eq} = 1.96 \times 10^6$ ,  $R_{eq,init} = 6.5 \times 10^3$ ; Test II:  $r''_{eq} = 2.83 \times 10^6$ ,  $R_{eq,init} = 8.9 \times 10^3$ ; Test III:  $r''_{eq} = 3.02 \times 10^6$ ,  $R_{eq,init} = 1.0 \times 10^4$ ; Test IV:  $r''_{eq} = 4.7 \times 10^6$ ,  $R_{eq,init} = 1.6 \times 10^4$ ; Test V:  $r''_{eq} = 19.9 \times 10^6$ ,  $R_{eq,init} = 6.8 \times 10^4$ .

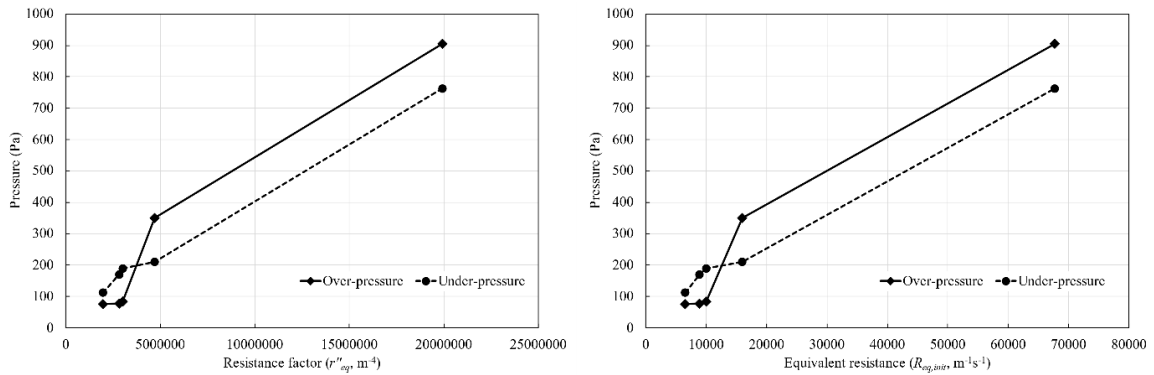


Fig. 16. Over-pressure and under-pressure peaks as function of resistance factor ( $r''_{eq}$ ) and initial equivalent resistance ( $R_{eq,init}$ ) in tests I-V.

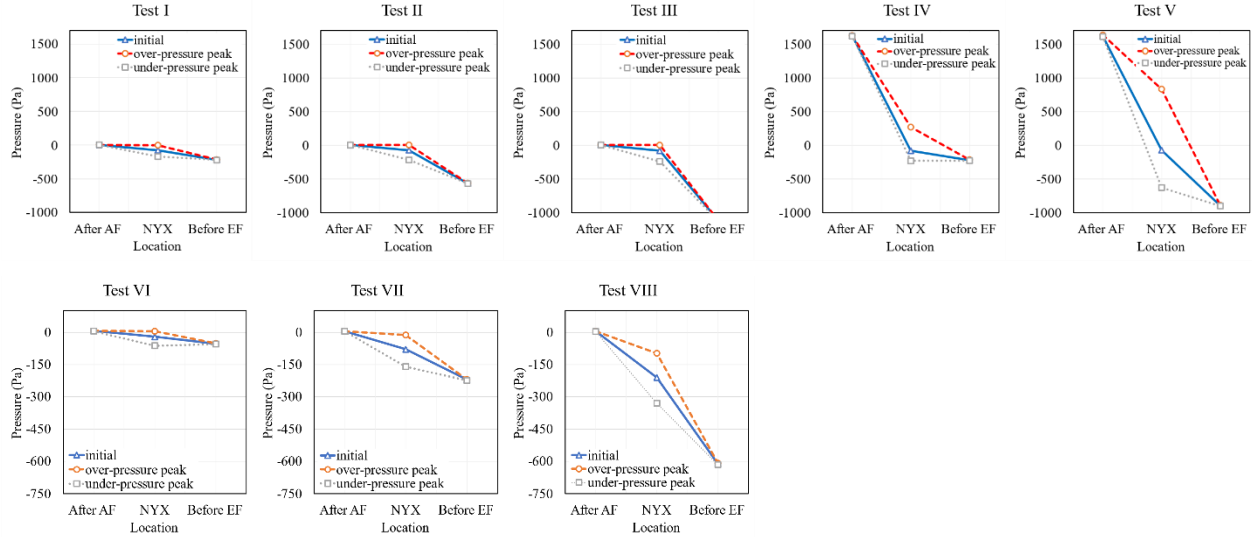


Fig. 17. Quantitative pressure changes along the ventilation ducts before fire (initial state) and during fire (over-pressure peak and under-pressure peak) at locations after the admission fan (AF), in the compartment (NYX) and before the extraction fan (EF).

In test IV, finally, the flow resistance in the admission duct is much higher than in the extraction duct. Consequently, the admission flow rate is not reduced significantly during the fire growth phase (Fig. 12). This leads to a significant rise in the compartment pressure, but less pronounced than in test V, because now the extraction flow rate is much higher (Fig. 12) due to the small flow resistance in the extraction duct in test IV, so the pressure does not build up as strongly as in test V. Another interesting observation for test IV is that the under-pressure in the decay phase is very comparable to what was observed in tests I-III (see Fig. 15). The reason is seen in Fig. 12: there is a very strong reduction in extraction flow rate in test IV, due to the low resistance in the extraction duct, in combination with a high resistance in the admission duct (so that the admission flow rate hardly changes, Fig. 12). As the temperatures are high at the start of the decay phase, there is a significant drop in heat and mass removal from the compartment due to the reduced flow rate in the extraction duct, counter-acting the pressure drop. Moreover, the activation of the strong admission fan in test IV also affects the pressure by blowing air into the compartment (mass inflow). As can be seen from Fig. 17, the pressure line changes significantly when the strong admission fan is activated in test IV. Thus, in the end, this leads to a pressure drop that is comparable to what was observed in tests I-III.

The above observations illustrate that the pressure variation is not only influenced by the thermal effect (the gain or removal of heat in the gas phase, driven by the fire HRR, and the thermal losses through the walls and the ducts), but also by the mechanical effect (the gain or removal of mass driven by the flows in the ventilation ducts), which is dependent on the flow resistances and fan operation.

### 3.3.2. Influence of the initial ventilation flow rate

Tests VI, VII, VIII are experiments with identical fire evolution and similar ventilation resistances (Table 4), but different initial ventilation flow rates are obtained by adjusting the extraction fan voltage. The corresponding air renewal rates are  $6.4 \text{ h}^{-1}$ ,  $12.8 \text{ h}^{-1}$  and  $21.3 \text{ h}^{-1}$ , respectively, for the tested initial ventilation flow rates of  $12 \text{ m}^3/\text{h}$ ,  $24 \text{ m}^3/\text{h}$  and  $40 \text{ m}^3/\text{h}$ . Fig. 18 reveals

qualitatively similar over-all pressure evolutions as tests I-V. Higher initial flow rates result in a more negative initial pressure, and to higher over-pressure and under-pressure peak values, despite the similar flow resistance caused by the valves ( $r''$  in Table 4). This can be understood from Fig. 19, showing the pressure evolution along the ventilation system before ignition: the static pressure decreases along the ventilation ducts until reaching the extraction fan, which raises the pressure back to ambient. The stronger the slope of the pressure line, the stronger the apparent resistance for flow in the ducts, explaining the higher pressure peaks for test VIII, compared to tests VI and VII. Interestingly, this effect is captured in the definition of  $R_{flow}$  (Eq. (7) and Table 4):  $R_{flow}$  is the lowest for test VI and the highest for test VIII. The under-pressure peak is also more pronounced with higher flow rates: more heat and mass are extracted from the compartment during the decay phase, in line with what has been explained above. Fig. 20 shows the pressure peaks as function of the resistance factor ( $r''_{eq}$ ) and total, or ‘equivalent’, flow resistance ( $R_{eq,init}$ ) for tests VI-VIII. The same results are obtained as discussed before, i.e., a higher equivalent flow resistance ( $R_{eq,init}$ ) leads to higher over-pressure and under-pressure peaks. This also illustrates the more or less linear increase of pressure with increase in equivalent flow resistance. Opposite trends are observed for the dependence of the pressure peaks on  $r''_{eq}$  and  $R_{eq,init}$  in Fig. 20. The reason is that, in fact, the relative difference between resistance factors in these cases is small (within 15%), and the main influencing factor in these cases is the initial ventilation flow rate, which is not included in the resistance factor.

Finally, it is noted in Fig. 20 that the over-pressure is lower than the under-pressure in these tests. This is in line with the analysis in section 3.3.1: the extraction fan ( $\Delta p_{EF}$ ) is always on, while the admission fan is off, resulting in higher under-pressure.

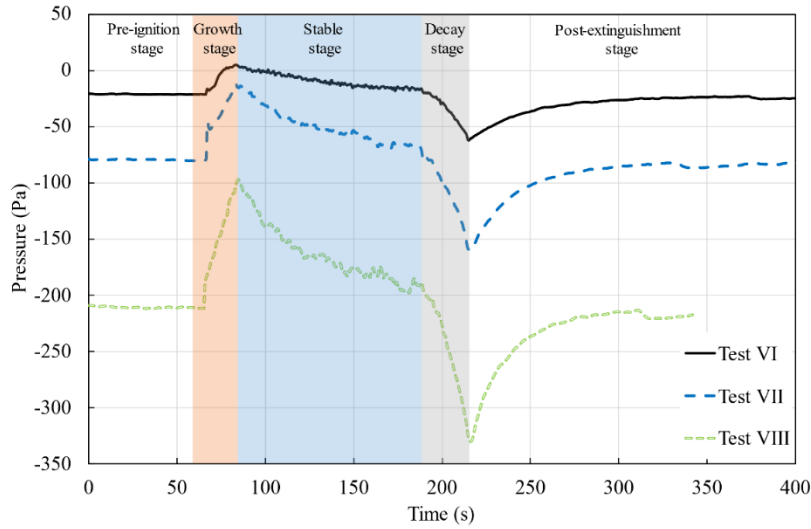


Fig. 18. Pressure variations as function of time in tests with different initial ventilation flow rates. Test VI:  $r''_{eq} = 2.13 \times 10^6$ ,  $R_{eq,init} = 3.6 \times 10^3$ ; Test VII:  $r''_{eq} = 1.97 \times 10^6$ ,  $R_{eq,init} = 6.6 \times 10^3$ ; Test VIII:  $r''_{eq} = 1.84 \times 10^6$ ,  $R_{eq,init} = 1.0 \times 10^4$ .

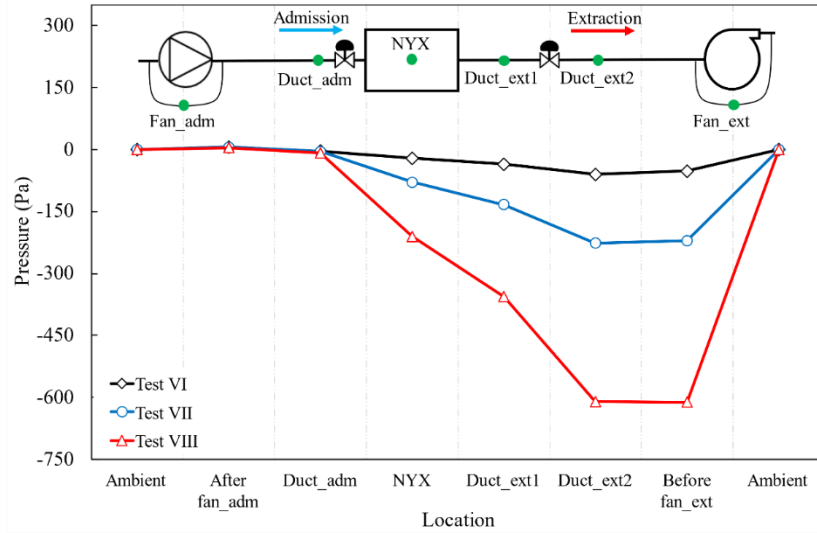


Fig. 19. Pressure changes along the ventilation system before fire ignition. Measuring points are marked in green dots on the top sketch. Note that the dots and other schematics just indicate the relative position, not refer to the actual scale.

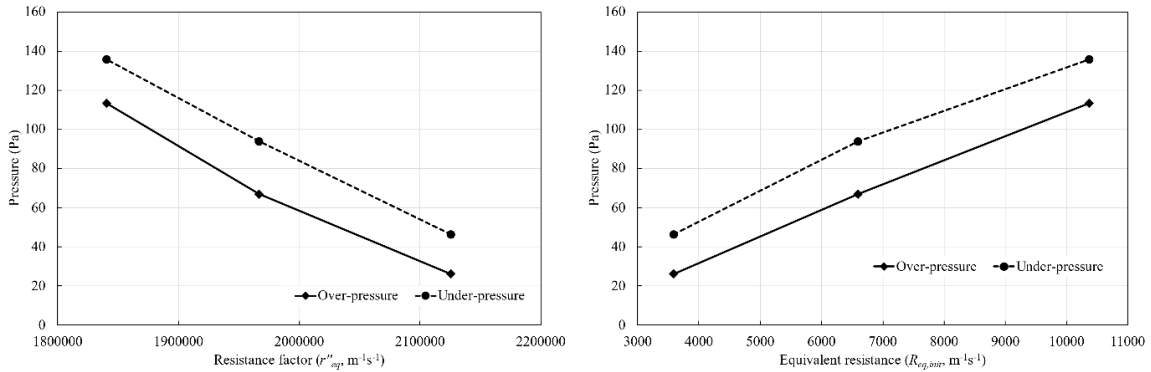


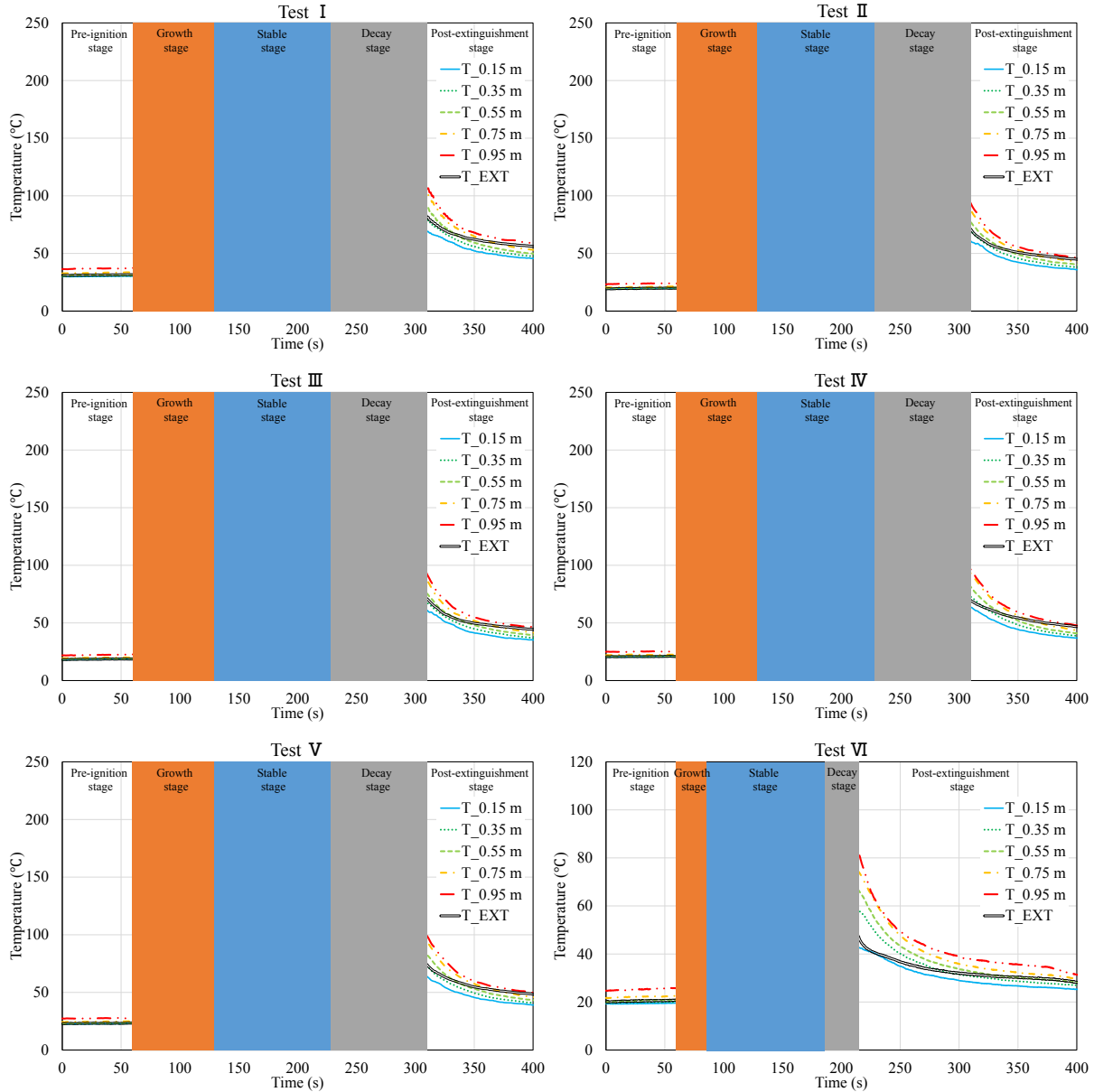
Fig. 20. Over-pressure and under-pressure peaks as function of resistance factor ( $r''_{eq}$ ) and initial equivalent resistance ( $R_{eq,init}$ ) in tests VI-VIII. Note that the relative differences between resistance factors are small (see Table 4).

### 3.4. The temperature profiles

The temperature measurements relate to the extraction of heat through the extraction duct and the heat losses through the boundary walls. The temperature evolutions as measured inside the compartment and in the extraction duct are shown as function of time in Fig. 21. As shown in Fig. 4, the gas temperatures at different heights are recorded at 4 positions (i.e., FL, FR, BL, BR). The temperature evolutions are similar at all 4 positions, hence, the temperatures at different heights shown in Fig. 21 are the average temperatures of the 4 positions. The results of tests I-V are very similar, indicating that the ventilation resistances have very little impact on the compartment temperature evolution for the configurations at hand. In tests VI-VIII the temperatures, especially in the upper layer, are affected by the ventilation flow rates: a higher initial flow rate leads to a higher air renewal rate of the compartment and thus lower temperatures. Yet,

comparing tests I-V to tests VI-VIII it is clear that the temperature evolution is essentially determined by the fire heat release rate.

It is also worth noting that the temperatures increase gradually, much slower than the pressure build-up in the fire growth phase. During the decay of the fire, the temperature also decreases more slowly than the fire HRR and the pressure drop. The temperatures are consequently much higher during the decay period than during the fire growth period, so that the heat losses through the walls (linked to the compartment temperature) and due to extraction through the ventilation system (linked to the temperature measured in the duct) play a more important role in the pressure variation during the fire decay period than during the fire growth stage.



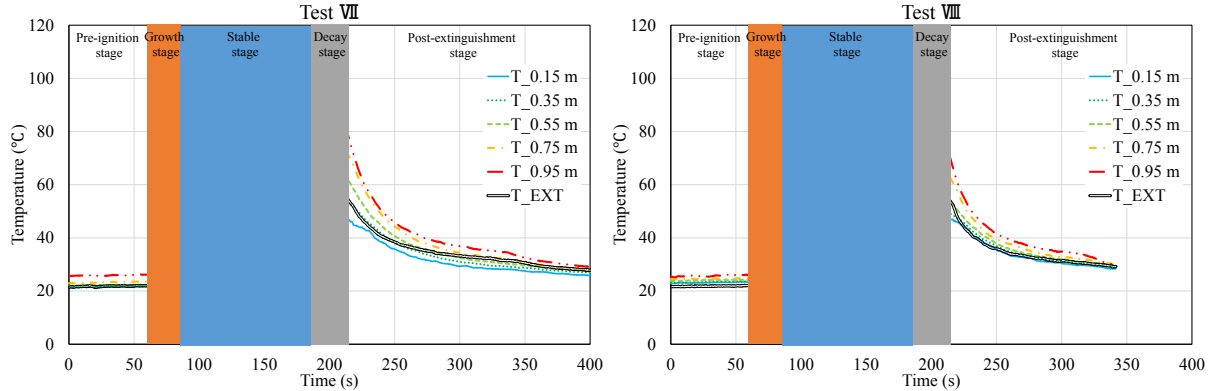


Fig. 21. Temperature evolutions as function of time at different heights (denoted by numbers in the legend) of the compartment and in the extraction duct (denoted by EXT in the legend).

#### 4. Conclusions

The effect of mechanical ventilation conditions and fire dynamics on pressure and temperature evolutions in an air-tight compartment has been discussed for a range of settings. The experimental set-up has been described in detail. The main end objective was the discussion of the evolution of pressure, imposing a fire with a quadratic growth, a steady and a quadratic decay phase, through well-controlled mass flow rate of propane, with variable ventilation conditions.

The over-all pressure evolution trends have been shown to be similar in the tests. Qualitatively, to first order the pressure follows the evolution of the fire HRR. However, the magnitudes of pressure peaks are strongly affected by the mechanical ventilation settings. Correspondingly, the fire-induced pressure has an influence on the ventilation flow rates.

Beyond the well-known outcome of higher pressure peak levels (over-pressure at the end of the growth phase and under-pressure at the end of the decay phase) for increased flow resistance in the ventilation system, it has been illustrated that not only the total, or ‘equivalent’, flow resistance is important, but also the individual flow resistances in the admission and extraction ducts separately.

The initial ventilation flow rate, or, equivalently, the imposed mechanical ventilation flow rate, strongly affects the pressure values. A higher imposed mechanical flow rate leads to a higher equivalent flow resistance (Eq. (7)) and hence higher over-pressure and under-pressure peak values.

The enhancement and reduction of ventilation flow rates depend on the fire-induced pressure, as well as the initial pressure difference in the ducts caused by resistance: flow rates vary more (respectively, less), depending on the pressure variation, as the flow resistance is lower (respectively, higher). The ratio between admission and extraction resistances leads to differences in flow variations in the admission and extraction ducts.

Finally, while the mechanical effect from the ventilation conditions has been illustrated to be important for the pressure evolutions, it hardly affects the temperature evolution (albeit that a cooling effect has been observed for the highest mechanical flow rate): the temperature evolution is essentially determined by the fire heat release rate and heat losses from the compartment.

## 5. Acknowledgements

The authors would like to thank Serge Pons, Julien Manzi, Vincent Lemaux and Paul Pelletier from IRSN for their support of the experiments. Thanks to the China Scholarship Council (CSC) for the financial support of Junyi Li (Grant No. 201706420076), as well as the co-funding from Ghent University through BOF (Grant No. 01SC2018).

## 6. Appendix: Analogy with electrical network

An analogy with electrical networks can be introduced in order to provide an explanation for the experimental observations. In this analogy:

- Voltage difference ( $\Delta V$ ) corresponds to pressure difference ( $\Delta p$ );
- Electrical charge ( $q$ ) corresponds to mass ( $m$ );
- Electrical current ( $I$ ) corresponds to mass flow rate ( $\dot{m}$ );
- Electrical resistance ( $R_{el}$ ) corresponds to flow resistance ( $R_{flow}$ );
- Electrical capacity ( $C$ ) corresponds to mass capacity ( $C_{mass}$ ).

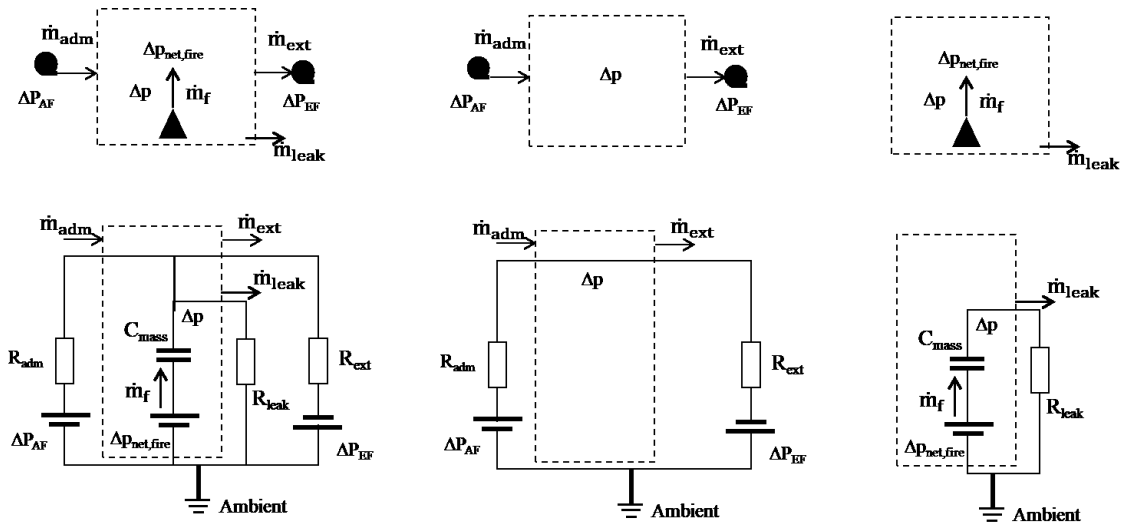


Fig. 22. Electrical network in analogy with the experiments. Left: general electrical network; middle: stable conditions prior to the fire, neglecting the leakage; right: situation if the compartment is disconnected from the mechanical ventilation network.

From the electrical analogue, namely that  $\Delta q = C\Delta V$ , and the ideal gas law, it can be derived that the ‘mass capacity’ (from a rise  $\Delta m$  in mass due to a pressure rise  $\Delta p$ ) reads:

$$C_{mass} = \frac{V}{TR} \#(19)$$

$R$  can be given the value of air ( $R = 287 \text{ J}/(\text{kg} \cdot \text{K})$ ), so Eq. (19) reveals that the mass capacity is proportional to the compartment volume  $V$ , and inversely proportional to the characteristic temperature,  $T$ , inside the compartment.

The next step is to define the flow resistance such that, as in electrical networks, the product  $R_{flow} C_{mass}$  has the unit of time (s). Knowing that the mass flow rate ( $\dot{m}$ ) is the analogue of the

electrical current  $I$  and that  $\Delta p$  is the analogue of electrical  $\Delta V$ , the equivalent flow resistance reads (cf. Ohm's law):

$$R_{flow} = \frac{\Delta p_{resis}}{\dot{m}} = \frac{r' \cdot v}{2A} = \frac{r' \cdot \dot{q}}{2} \#(20)$$

## 7. References

- [1] Schnieders J, Feist W, Rongen L, Passive Houses for Different Climate Zones, Energy and Buildings. 105 (2015) 71-87. <https://doi.org/10.1016/j.enbuild.2015.07.032>
- [2] Prignon M, Van Moeseke G, Factors Influencing Airtightness and Airtightness Predictive Models: A Literature Review, Energy and Buildings. 146 (2017) 87-97. <https://doi.org/10.1016/j.enbuild.2017.04.062>
- [3] Pretrel H, Le Saux W, Audouin L, Pressure Variations Induced by a Pool Fire in a Well-Confined and Force-Ventilated Compartment, Fire Safety Journal. 52 (2012) 11-24. <https://doi.org/10.1016/j.firesaf.2012.04.005>
- [4] Pretrel H, Such JM, Effect of Ventilation Procedures on the Behaviour of a Fire Compartment Scenario, Nuclear Engineering and Design. 235 (2005) 2155-2169. <https://doi.org/10.1016/j.nucengdes.2005.03.003>
- [5] Hostikka S, Janardhan RK, Riaz U, Sikanen T, Fire-Induced Pressure and Smoke Spreading in Mechanically Ventilated Buildings with Air-Tight Envelopes, Fire Safety Journal. 91 (2017) 380-388. <https://doi.org/10.1016/j.firesaf.2017.04.006>
- [6] Janardhan RK, Hostikka S, Experiments and Numerical Simulations of Pressure Effects in Apartment Fires, Fire Technology. 53 (2017) 1353-1377. <https://doi.org/10.1007/s10694-016-0641-z>
- [7] Audouin L, Rigollet L, Pretrel H, Le Saux W, Rowekamp M, OECD PRISME Project: Fires in Confined and Ventilated Nuclear-Type Multi-Compartments - Overview and Main Experimental Results, Fire Safety Journal. 62 (2013) 80-101. <https://doi.org/10.1016/j.firesaf.2013.07.008>
- [8] Utiskul Y, Quintiere JG, Rangwala AS, Ringwelski BA, Wakatsuki K, Naruse T, Compartment Fire Phenomena under Limited Ventilation, Fire Safety Journal. 40 (2005) 367-390. <https://doi.org/10.1016/j.firesaf.2005.02.002>
- [9] Chow WK, Zou GW, Numerical Simulation of Pressure Changes in Closed Chamber Fires, Building and Environment. 44 (2009) 1261-1275. <https://doi.org/10.1016/j.buildenv.2008.09.016>
- [10] Karlsson B, Quintiere J, Enclosure Fire Dynamics, CRC press, 1999. 114
- [11] Li J, Beji T, Brohez S, Merci B, Experimental and Numerical Study of Pool Fire Dynamics in an Air-Tight Compartment Focusing on Pressure Variation, Fire Safety Journal. (2020) 103128. <https://doi.org/10.1016/j.firesaf.2020.103128>
- [12] Li J, Beji T, Brohez S, Merci B, CFD Study of Fire-Induced Pressure Variation in a Mechanically-Ventilated Air-Tight Compartment, Fire Safety Journal. (2020). <https://doi.org/10.1016/j.firesaf.2020.103012>
- [13] Rehm RG, Forney GP, The Pressure Equations in Zone-Fire Modeling, Fire Science and Technology. 14 (1994) 61-73. <https://doi.org/10.3210/fst.14.61>
- [14] Quintiere JG, Fundamentals of Fire Phenomena, John Wiley & Sons Ltd, 2006. 232
- [15] Laverge J, Pattyn X, Janssens A, Performance Assessment of Residential Mechanical Exhaust Ventilation Systems Dimensioned in Accordance with Belgian, British, Dutch, French and Ashrae Standards, Building and Environment. 59 (2013) 177-186. <https://doi.org/10.1016/j.buildenv.2012.08.018>
- [16] Institute PH, Passive House Requirements. [https://passivehouse.com/02\\_informations/02\\_passive-house-requirements/02\\_passive-house-requirements.htm](https://passivehouse.com/02_informations/02_passive-house-requirements/02_passive-house-requirements.htm), (accessed 26 April 2020).
- [17] Jiang F, Ye SS, Yang J, Design of the Exhaust System in the Confinement of the Htr-10, Nuclear Engineering and Design. 218 (2002) 209-214. [https://doi.org/10.1016/S0029-5493\(02\)00192-9](https://doi.org/10.1016/S0029-5493(02)00192-9)

- [18] Mense M, Pizzo Y, Prétrel H, Lallemand C, Porterie B, Experimental and Numerical Study on Low-Frequency Oscillating Behaviour of Liquid Pool Fires in a Small-Scale Mechanically-Ventilated Compartment, *Fire Safety Journal*. 108 (2019) 102824. <https://doi.org/10.1016/j.firesaf.2019.102824>
- [19] EN ISO 9972:2015 Thermal Performance of Buildings-Determination of Air Permeability of Buildings-Fan Pressurization Method. European Committee for Standardization, Brussels, 2015.
- [20] Beji T, Merci B, Assessment of the Burning Rate of Liquid Fuels in Confined and Mechanically-Ventilated Compartments Using a Well-Stirred Reactor Approach, *Fire Technology*. 52 (2016) 469-488. <https://doi.org/10.1007/s10694-014-0418-1>
- [21] Alvares NJ, Foote KL, Pagni PJ, Forced Ventilated Enclosure Fires, *Combustion Science and Technology*. 39 (1984) 55-81. <https://doi.org/10.1080/00102208408923783>